

B.K. Ostafiychuk, M.I. Kolkovskiy, B.I. Rachiy, P.I. Kolkovskiy,
N.Ya. Ivanichok, R.V. Ilnitsky

Accumulation Charge Mechanisms in Electrochemical Systems Formed Based on Activated Carbon and Manganese Oxide

Vasyl Stefanyk Precarpathian National University, Ivano-Frankivsk, Ukraine, e-mail: Pkolkovskyy@gmail.com

In this work, the porous structure of the carbon material and the crystalline structure of manganese oxide α -modification (α -MnO₂) have been investigated. The electrochemical performance of symmetric and asymmetric supercapacitors (α -MnO₂/Activated carbon) was investigated by cyclic voltammetry and galvanostatic cycling methods. The processes occur mainly at the electrode–electrolyte interface have been analyzed. It was determined that at discharge currents of 0.5–5 mA, the specific capacitance value for the α -MnO₂. Activated carbon hybrid capacitor exceeds the value of the symmetric capacitor by 45–55 % under the same conditions.

Keywords: hybrid electrochemical supercapacitors, porous carbon material, manganese oxide.

Received 12.02.2020; accepted for publication 15.03.2020.

Introduction

Nowadays, the development of high-efficiency electrochemical devices based on charge accumulation is an actual task. One of the most promising direction is the design devices with high performance $> 10^6$ charges / discharge cycles stable Coulomb efficiency. Electrochemical capacitors (ECs) are such type devices which accumulated energy is due to redox reactions and the formation of an electric double layer capacitors (EDLCs), which is formed at the interface of the electrode material/electrolyte based on a large specific surface area (1500 - 2000 m²/g) [1]. In many cases, the formation of final phase and irreversible changes of electrode are based on the redox reactions that are responsible for the accumulation of charge. Thus, the urgent task is to obtain new electrode materials that do not break down or degrade during charge/discharge process [2, 3].

Activated carbon (AC) is one of the most common materials for electrodes of classical ECs. Moreover, supercapacitors, which were fabricated from AC, is operating on the charge / discharge process of EDL [4]. Therefore, the high capacity ECs are implemented based on AC electrodes. Advantages of application AC in EC are simple obtaining procedure, high specific energy

characteristics, chemical stability, as well as the availability of raw materials and its cheapness. However, the insufficiently high accumulated specific energy of EC compares with power sources encourages the search new solutions to this problem. Thus, one of the options for increasing specific energy is the formation of hybrid capacitor systems (HC). Hybrid capacitors are use electrodes with different characteristics such as electrostatic and electrochemical capacitance [5]. The EC based on a non-polarized electrode is cause the increases of the voltage of a single element increases the operating window of the voltage of the EC and its total capacitance. Since, a second series-connected capacitor is removed from the equivalent circuit [6]. Therefore, due to the implementation of 2 different mechanisms of charge storage, HCs can fill the efficiency gap between the energy density of batteries and the high power density of conventional dielectric capacitors, and thus provide fast energy storage and release [7].

On the one hand, activated carbon material is used for a polarized electrode. On the other hand, the oxides, hydroxides and sulfides of transition metals used are promising materials for unpolarized electrode.

In this work, the porous structure of carbon material was research as well as, the crystal structure of type α -MnO₂, and the electrochemical characteristics of

symmetric and asymmetric supercapacitors with electrodes based on them.

I. Experimental details

The polarized electrode had been formed based on carbon material, which previously was experimentally obtained by carbonization and thermochemical activation with potassium hydroxide of raw materials of natural origin [8, 9].

The characteristics of the porous structure (surface area and total pore volume) of the carbon material were determined based on the analysis of nitrogen adsorption/desorption isotherms at boiling point (77 K) by Quantachrome Autosorb Nova 2200e instrument. Additionally, the samples were previously degassed at 450 K for 18 h. The characteristics of the porous structure of carbon materials were determined by analyzing the adsorption/desorption isotherms. Namely, the total surface area (S_{BET}) by the BET multipoint method in the isotherm limited by the relative pressure range $P/P_0 = 0.050 \dots 0.35$, the total pore volume (V_{total} , cm^3/g) calculated by the amount of sorbet nitrogen at $P/P_0 \sim 1$.

Monophasic mesoporous of type α - MnO_2 with predetermined morphology was obtained based on the redox reaction $3\text{MnCl}_2 + 2\text{KMnO}_4 + 2\text{H}_2\text{O} \rightarrow 5\text{MnO}_2 + 4\text{HCl} + 2\text{KCl}$ by hydrothermal route. Reagents for the synthesis of α - MnO_2 were used aqueous solutions of 0.04 M of KMnO_4 , 0.06 M of MnCl_2 and 4 M cationic impurity KCl.

The electrodes of the EC ($m = 0,25$ g) were performed based on the active material 85 %, conductive material 10 % and 5 % polyvinylidene fluoride mixed with *n*-methylpyrrolidone and dried at 80°C for 3 hours. Then, hybrid supercapacitor has been formed. A mixture of active materials was used as a electrode, which was placed in a nickel cell of a 2032 size. KOH was used as an electrolyte 33 % of aqueous solution. Electrochemical studies were performed an Autolab PGSTAT/FRA-2 spectrometer in galvanostatic and potentiodynamic modes. The charge / discharge measurements were done at current values of 0.5, 100 mA. Cyclic voltammetry measurement were performed at scan rates of 1, 100 mV/s.

II. Results and discussion

2.1. Investigation of carbon material and manganese oxide structures.

Nitrogen adsorption - desorption isotherms of carbon materials are shown in Fig. 1. The volume of sorbet nitrogen increases to $450 \text{ cm}^3/\text{g}$ with an increase in relative pressure to 1 and gradually decreases during desorption, forming a hysteresis loop at high pressures.

The hysteresis loop can be classified as type H4 according to the IUPAC classification [10], which is associated with capillary condensation in mesopores. The growth of the adsorption area of the isotherm near $P/P_0 = 1$ is caused by multiple processes of nitrogen condensation and evaporation in situ meso and

macropores. The width of the hysteresis probably corresponds to the amount of adsorbate in the blocked meso and macropores. Moreover, the volume of the mesopores was calculated from the hysteresis value. Quantitative characteristics of the porous structure of the obtained AC were determined based on the analysis of adsorption/desorption isotherms (Fig. 1). To compare the specific surface area of AC, a number of complementary methods were used: BET, Langmuir (L-method), t-method, DR, BJH and DFT (Table 1.). The value of specific surface area was determined using the BET method with a linear graph of $1/[W(p_0/p) - 1]$ versus p_0/p in the adsorption isotherm range for the p_0/p ratio in the range from 0.05 to 0.35 [11]. To investigation the structure of microporous carbon materials, it is also advisable to use the Langmuir method [12], DFT [13], and the t - method [14], since the BET method does not completely take into account the contribution of micropores [10].

As a result, the obtained carbon material is microporous with mesopores constituting up to 15 % of the total surface area. A surface area of $1236 \text{ m}^2/\text{g}$ is determined by three methods; it correlates within the error margin of 10%. The micropore volume determined by the t-method is $0.41 \text{ cm}^3/\text{g}$, which is about 60 % of the total pore volume determined at maximum pressure. The obtained carbon material owns a highly developed surface area of 1100 - 1300 m^2/g and micro- and mesoporous structure. Mesopores are type transport channels for adsorbate or electrolyte to enter micropores. The distribution of the area and pore volume by the size of the investigated AC obtained by the DFT method using the model of slit-like pores is shown in Fig. 2.

From the distribution of volume and pore area by size (Fig. 2a), it can be seen that micropores with a size of 0.5 - 2 nm introduce a significant contribution to the specific surface area and the total pore volume. The mesopores about 2 - 6 nm in size form (Fig. 2b) a porous volume of $0.28 \text{ cm}^3/\text{g}$ (Table 1).

XRD patterns of the MnO_2 obtained by hydrothermal synthesis method at a temperature of 180°C for 48 hours Fig. 3. The monophasic ultrafine form of α - MnO_2 phase (JCPDS no.42-1348) with a crystal structure of Mn^{4+} and O^{2-} , was successfully formed. The average sizes of

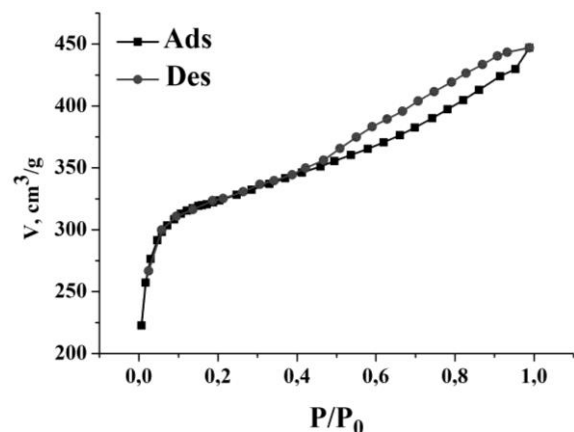
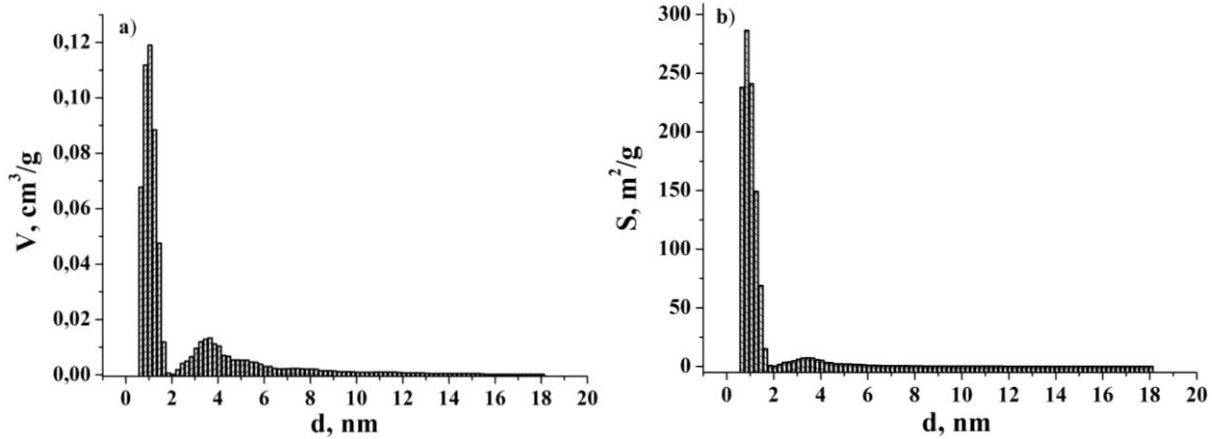


Fig. 1. Isotherms of nitrogen adsorption/desorption of AC.

Table 1

Sorption characteristics of AC

Material	S_{BET} , m^2/g	S_L , m^2/g	S_{DFT} , m^2/g	$S_{I-micro}$, m^2/g	$S_{BJH-meso}$, m^2/g	S_{micro} , %	V_{total} , cm^3/g	V_{micro} , cm^3/g
AC	1236	1405	1085	1040	160	84	0,69	0,41

**Fig. 2.** The distribution of volume and pore area by size of AC.

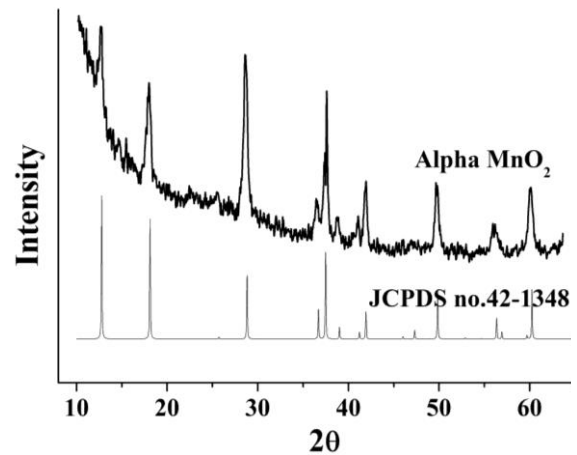
coherent scattering domains (CSD) was calculating based on Sherrer's equation. Thus, the average sizes of the CSD are 12 - 16 nanometers. As a result, the 4M concentration of KCl ions is a key factor in the formation of the α - MnO_2 phase.

2.2. Electrochemical parameters of symmetric and asymmetric supercapacitors.

The typical shape of the curves at scan rates of 2 - 10 mV/s is close to rectangular. This is typical for ECs with EDL for the symmetric capacitor AC / AC (Fig. 4a). The increase of charge / discharge passage processes reduces the availability and movement of electrolyte ions into the electrode material is due to an increase in the scan rates to 20 - 50 mV/s (Fig. 4,b). In this case, the effective interaction between the electrolyte ions and the electrode is significantly reduced due to the resistance of the electrode materials, and is reflected in the deviation of the cyclic voltammogram from a rectangular shape. The obtained potentiodynamic curves have a symmetrical shape, which indicates quasi-reversal of the charge / discharge of the EDL.

The discharge curves of the symmetric supercapacitor AC / AC have the form of straight lines without a plateau. That fact is confirms the data of CVA investigation and indicates the predominant contribution of EDL charge accumulation process (Fig. 5).

The specific capacitance of the symmetric supercapacitor AC / AC is 32,9 F/g at a discharge current of 5 mA (Fig. 5, a) The obtained value is determined from the obtained galvanostatic curves. However, the specific capacitance is decrease to 24,5 F/g with increasing discharge currents to 100 mA (Fig. 5, b). Thus, it can be concluded that in with an increase in the discharge current in the carbon material, the equivalent series resistance increases (limited by diffusion in micropores [15]). As a result, access to the inner surface

**Fig. 3.** XRD patterns of the obtained sample and reference (JCPDS no.42-1348) α - MnO_2

of the material is limited. Potentially dynamic curves for the hybride supercapacitor α - MnO_2 / AC are shown in Fig. 6. The curves were obtained preserving a potential window of 1 V at a scan rate of 1 mV/s. The obtained CVA curves (Fig. 6) are characterized by the presence of redox peaks. Moreover, the presence of redox peaks is a confirmation that redox reactions occur, mainly according to the scheme of $Mn^{3+} \leftrightarrow Mn^{4+}$.

To investigation the stability of the asymmetric EC operation, the voltage range was increased to 1.4 V compared to the symmetric one (Fig. 7).

The obtained values of specific capacities, which were calculated from the CVA curves, are 26.1, 34.3 and 48.38 F/g, according to the potentials range 0 - 1, 0 - 1.2, 0 - 1.4 V. Then, potentiodynamic and galvanostatic investigation were carried out in a potential range of 0 - 1.4 V. High rates of electronic and ionic charge transfer mechanisms are observed with an increase in the scan

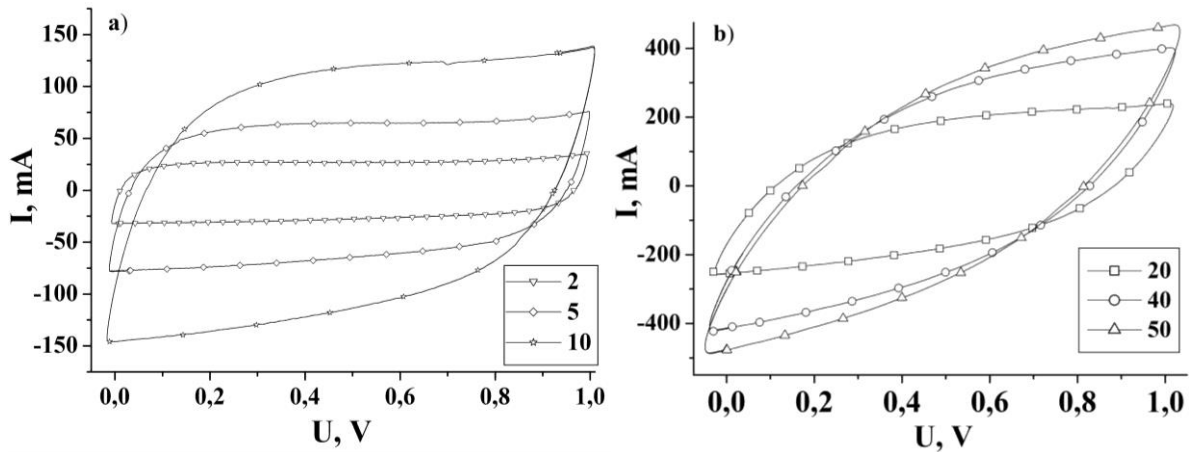


Fig. 4. CVA curves of the symmetric capacitor AC / AC with a scan rate of 2 - 10 mV/s (a), 20 - 50 mV/s (b).

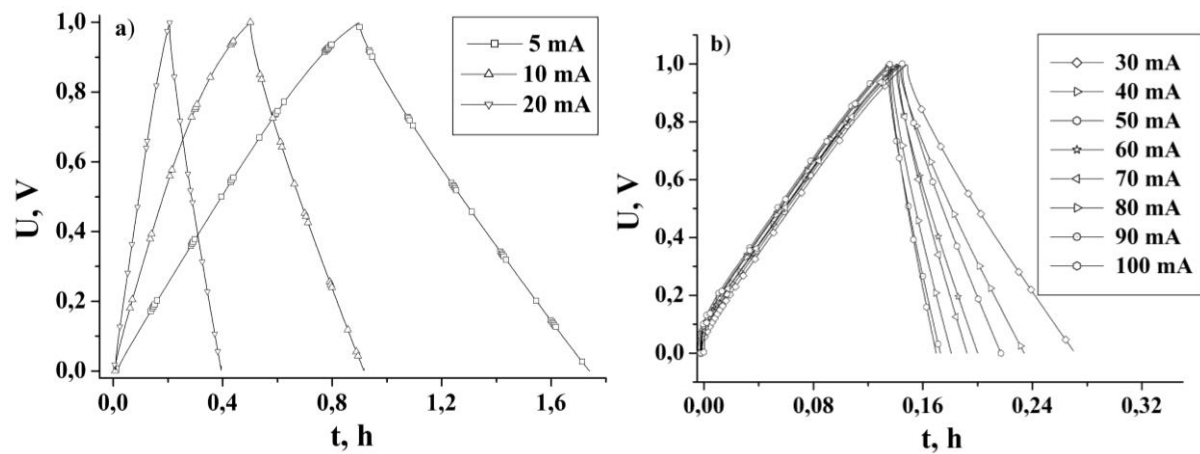


Fig. 5. The charge-discharge curves of the EC AC/AC.

rate to 50 mV/s.

That is proved by recorded of redox peaks on the CVA curves (Fig. 8). There is a proportional increase in the peak region, which indicates the reversibility of the kinetic process [11].

Figure 9 shows the dependence of the capacitance on the discharge current and the scan rate for EC AC / AC

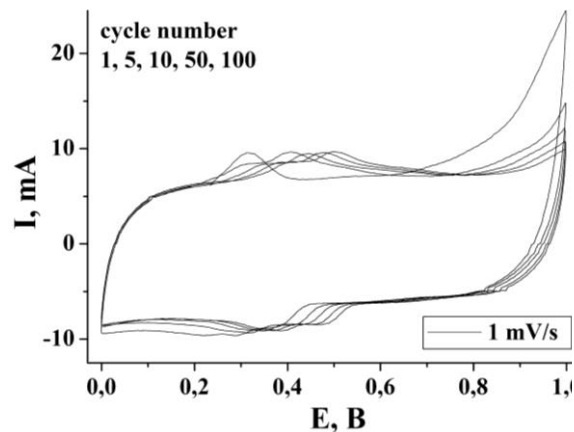


Fig. 6. The CVA curves of an asymmetric α -MnO₂ / AC supercapacitor with a scan rate at 1 mV/s a) after 1, 5, 10, 50 and 100 cycles.

and HC α -MnO₂ / AC. At low discharge currents up to 10 mA, the specific capacitance of the HC is one and a half times greater than the suitable capacity of a symmetric EC. The increase discharge current (Fig. 9a) and scan rate (Fig. 9,b) leads to a gradual decrease in the specific capacitance of both investigated EC models. The monotonic decrease in the specific capacity of symmetric EC can be explained by the mobility of ions within certain micropores (especially the surface of micropores, partially accessible to electrolytes). At relatively high charge / discharge speeds, EDL within the ultramicropores and micropores is not completely formed. With an increase in scanning speed, the number of these inaccessible micropores increases, internal resistance increases, and accordingly, a monotonic decrease in specific capacitance is observed. For a HC at low scanning rates, redox reactions have time to occur, and therefore an accumulation of electric charge is ensured. The high scan rate or short time is lead to a sharp decrease in charge accumulation. It is due to the redox reactions that should have taken place do not occur to the end.

The total capacity of materials can be divided into two components accordance with Figure 9b. On the one hand is capacity of double electric layer. And, on the other hand is diffusion-controlled oxidation-reduction

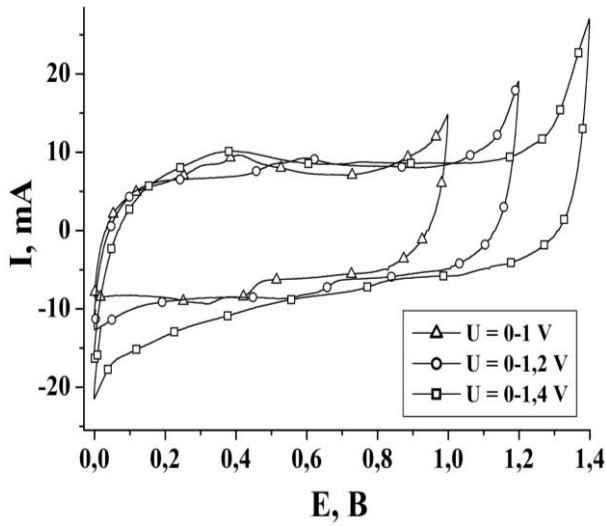


Fig. 7. The CVA curves of an asymmetric α - MnO_2 / AC supercapacitor from 0 to 1.4 V with a scan rate at 1 mV/s.

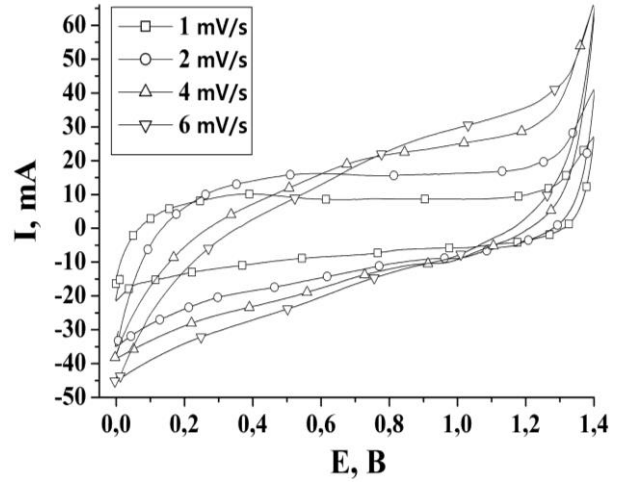


Fig. 8. The CVA curves of an asymmetric α - MnO_2 / AC supercapacitor from 0 to 1.4 V with a scan rate at 1, 2, 4 and 6 mV/s.

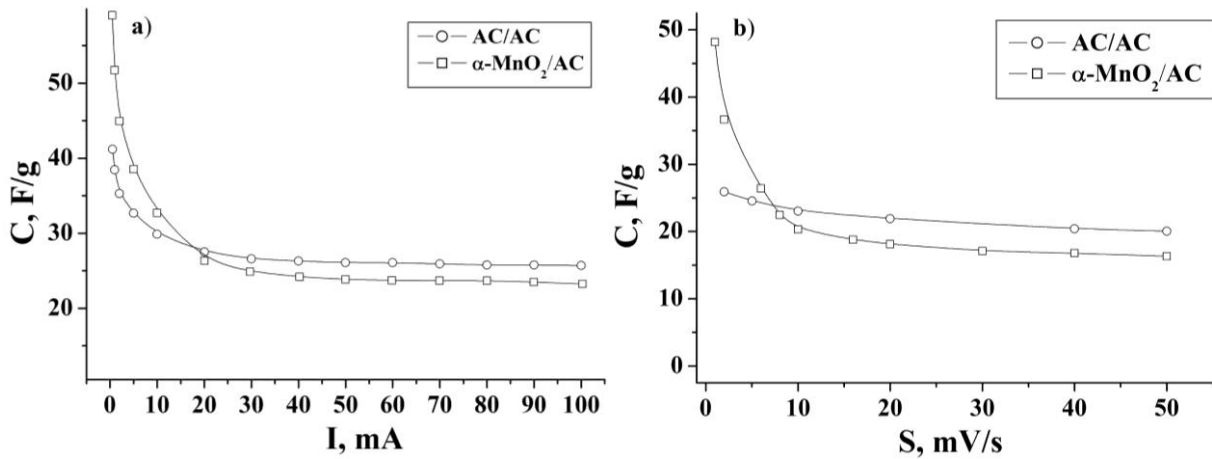


Fig. 9. Dependence of specific capacitance on discharge current a) and scan rate b) for AC / AC - EC and α - MnO_2 / AC - HC.

capacity due to fast reverse faraday reactions (C_F) $C = C_{EDL} + C_F$ [15]. Nevertheless, it has been suggested that in the kinetic model [16], the scan rate affects the total specific electrochemical capacity of the system. Since, the diffuse component of the capacitance is a function of the reaction time. So, the scan rate can be considered inverse to the time of diffusion. Thus, in the case of a semi-infinite linear diffusion, the total capacity is related to the scan rate by the following equation $C = C_{s=\infty} + a / \sqrt{s}$. Were, a is constant and $C_{EDL} = C_{s=\infty}$.

Determination of the specific capacity of EDL of the investigated materials (table. 2) is possible due to extrapolation of the C dependencies from $s^{1/2}$ to the Y-axis (Fig. 10, a).

The increase in specific capacity is due to a decrease in the scanning speed (Fig. 10, b). Thus, the dependence of the specific capacity on the scanning speed can be

extrapolated to the other side to $s = 0$ using the functional dependence on s [16].

Since, C is increases linearly with $s^{-1/2}$, then $1/C$ should decrease linearly with $s^{1/2}$. Then, $1/C = 1/C_{s=0} = b\sqrt{s}$ where $C_{s=0}$ is the maximum specific capacity that can be obtained and b is a constant. The magnitude inverse of specific capacity is linearly dependent on $s^{1/2}$, as can be seen from Fig. 10, b. The maximum specific capacity of the investigated materials was determined based on of extrapolation of the dependence of C^{-1} on $s^{1/2}$ of the Y axis (Fig. 10, b) (Table 2). Additionally, the nonlinear nature of the galvanostatic curves is a confirmation of the pseudo-capacitance behavior of the HC (Fig. 11). The formed voltage plateaus are in good agreement with the peaks observed on the corresponding CVA.

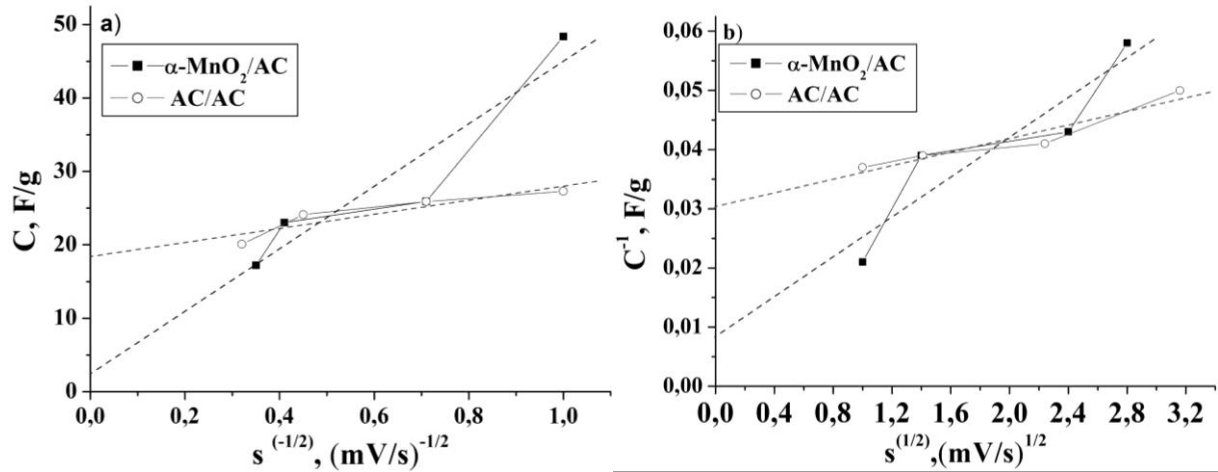


Fig.10. Dependence of C on $s^{-1/2}$ a) and $1/C$ on $s^{1/2}$ b) for EC and HC.

Table 2

Specific characteristics of symmetrical and hybrid capacitors

Capacitor type	AC / AC	$\alpha - \text{MnO}_2 / \text{AC}$
$C_{\text{EDL}}, \text{F/g}$	18,5	2,23
$C_{\text{max}}, \text{F/g}$	32,26	116,28
$C_{\text{EDL}}/C_{\text{max}}$	0,574	0,019

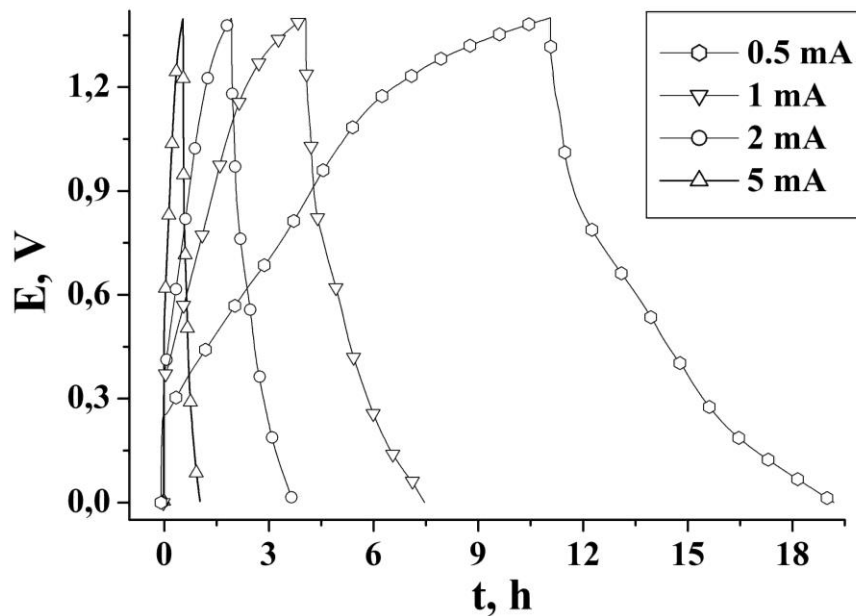


Fig. 11. Charge-discharge curves of a $\alpha - \text{MnO}_2 / \text{AC}$ HC.

At discharge currents of 0.5 - 5 mA, the specific capacitance value for the $\alpha - \text{MnO}_2 / \text{AC}$ asymmetric capacitor exceeds the value of the symmetric capacitor

by 45 - 55 % under the same conditions.

Conclusions

It was determined that hybrid supercapacitor is characterized by better electrochemical performances compared to symmetric due to structural properties of electrode material.

On the one hand, the porous carbon structure guarantees a high specific surface area (up to $1250 \text{ m}^2 \text{ g}^{-1}$) with an average pore size of 2–6 nm, which increases the electrode/electrolyte contact region, and as well as opens up additional possibilities for the passage of fast Faraday reverse reactions. On the other hand, the layered structure of manganese oxide α -modification with the average sizes of coherent scattering regions of 12–16 nanometers determined according to the Scherrer formula provides fast ionic and electronic charge transfer mechanisms and provides a cyclical process, and therefore leads to a high specific capacity formed on its

basis laboratory models of electrochemical capacitors.

Ostafiychuk B.K. - Doctor of Sciences, Professor, Head of the Department of Material Science and New Technology;

Kolkovskiy M.I. – PhD student, of the Department of Material Science and New Technology;

Rachiy B.I. - Doctor of Sciences, Professor, of the Department of Material Science and New Technology;

Kolkovskiy P.I. – Doctoral student of the Department of Material Science and New Technology;

Ivanichok N.Ya – PhD, senior specialist of the Department of Material Science and New Technology;

Ilnitsky R.V. - Doctor of Sciences, Professor, of the Department of Material Science and New Technology.

- [1] B.E. Conway, *Electrochemical Supercapacitors: Scientific Fundamentals and Technological Applications* (N.Y. Kluwer Academic Plenum Publishers, 1999).
- [2] B.K. Ostafiychuk, R.P. Lisovskiy, A.H.Z. Al-Saedi, B.I. Rachiy, V.O. Kotsyubynsky, P.I. Kolkovskiy, R.I. Merena, A.B. Hrubciak, *Journal of Nano- and Electronic Physics* 11(3), 03036 (2019) ([https://doi.org/10.21272/jnep.11\(3\).03036](https://doi.org/10.21272/jnep.11(3).03036)).
- [3] R. Lisovsky, B. Ostafiychuk, I. Budzulyak, V. Kotsyubynsky, A. Boychuk, B. Rachiy, *Acta Physica Polonica A*. 133(4), 876 (2018). (<https://doi.org/10.12693/APhysPolA.133.876>).
- [4] A.I. Kachmar, V.M. Boichuk, I.M. Budzulyak, V.O. Kotsyubynsky, B.I. Rachiy & R.P. Lisovskiy, *Fullerenes, Nanotubes and Carbon Nanostructures* 27(9), 669 (2019) (<https://doi.org/10.1080/1536383X.2019.1618840>).
- [5] B. Conway, W. Pell, *Proceedings of the 12-th International Seminar on DLC and Similar Energy Storage Devices* (Deerfield Beach, Florida, USA, 2002).
- [6] A.I. Belyakov, *The 6-th International Similar on DLC and Seminar Energy Storage Devices* (Deerfield Beach, Florida, USA, 1996).
- [7] J. Miller, P. Simon, *Science* 321(5889), 651 (2008) (<https://doi.org/10.1126/science.1158736>).
- [8] L. Zhang, X. Zhao, *Chemical Society Reviews* 38(9), 2520 (2009) (<https://doi.org/10.1039/B813846J>).
- [9] B.K. Ostafiychuk, I.M. Budzulyak, B.I. Rachiy, V.M. Vashchynsky, V.I. Mandzyuk, R.P. Lisovsky and L.O. Shyyko, *Nanoscale Research Letters* 10(1), 65 (2015) (<https://doi.org/10.1186/s11671-015-0762-1>).
- [10] A.P. Karnaukhov, *Adsorption. The texture of dispersed and porous materials* (Novosibirsk, Science, Sib. enterprise RAN Publ, 1999).
- [11] S. Brunauer, P. Emmett, E. Teller, *Journal of the American Chemical Society* 60(2), 309 (1938) (<https://doi.org/10.1021/ja01269a023>).
- [12] A.V. Kiselev, *Surface phenomena. Adsorption* (Moscow, Chemistry, 1969).
- [13] NOVA operating manual (Quantachrome Instruments, 2010).
- [14] T.G. Plachenov, S.D. Kolosencev, *Porometriya* (Leningrad, Chemistry, 1988).
- [15] H. Wang, L. Pilon, *Electrochimica Acta* 64(1), 130 (2012) (<https://doi.org/10.1016/j.electacta.2011.12.118>).
- [16] S. Ardizzone, G. Fregonara, S. Trasatti, *Electrochimica Acta* 35(1), 263 (1990) ([https://doi.org/10.1016/0013-4686\(90\)85068-X](https://doi.org/10.1016/0013-4686(90)85068-X)).

Б.К. Остафійчук, М.І. Колковський, Б.І. Рачій, П.І. Колковський,
Н.Я. Іванічок, Р.В. Ільницький

Механізми накопичення заряду в електрохімічних системах, сформованих на основі вуглецю і оксиду марганцю

*ДВНЗ “Прикарпатський національний університет імені Василя Стефаника”, Івано-Франківськ,
Україна, e-mail: Pkolkovskyu@gmail.com*

В даній роботі проведено дослідження пористої структури вуглецевого матеріалу та кристалічної структури оксиду марганцю α – модифікації (α - MnO_2). Методами хроноамперометрії та вольтамперометрії досліджено електрохімічну поведінку симетричного (Активований вуглець / Активований вуглець) та асиметричного суперконденсаторів (α - MnO_2 / Активований вуглець). Проаналізовані процеси, що відбуваються на межі розділу фаз електродів. Показано, що при струмах розряду 1 і 5 мА значення питомої ємності для гібридного конденсатора α - MnO_2 / Активований вуглець перевищує дане значення для симетричного конденсатора на 45 - 55 % при цих умовах.

Ключові слова: гібридні електрохімічні суперконденсатори, пористий вуглецевий матеріал, оксид марганцю.